










Phenylboronic acid-functionalized ultra-pH-sensitive micelles for enhanced tumor penetration and inhibition in vitro

Jiejie Qin¹ , Yan Huang¹ , Guoqing Yan¹ , Jun Wang¹ , Liefeng Hu¹ , Panpan Zhang¹ , and Rupei Tang^{1,*} 

¹ Engineering Research Center for Biomedical Materials, Anhui Key Laboratory of Modern Biomanufacturing, School of Life Sciences, Anhui University, 111 Jiulong Road, Hefei 230601, Anhui Province, People's Republic of China

Received: 1 September 2018

Accepted: 30 October 2018

Published online:

2 January 2019

© Springer Science+Business Media, LLC, part of Springer Nature 2019

ABSTRACT

In this work, the tumor-targeted ultra-pH-responsive conjugates (PBA/Dex-g-OE) and nontargeted conjugates (Dex-g-OE) were successfully prepared and could easily self-assemble into stable micelles with lower CMC values in neutral aqueous solution. Transmission electron microscopy and dynamic light scattering measurement indicated that the resulting micelles have desirable size distribution and regular spherical shape. The PBA/Dex-g-OE micelles possessed high stability in physiological condition and were pH sensitive to both extracellular and intracellular acidic conditions. Doxorubicin (DOX) was efficiently loaded to give the DOX-loaded micelles (PBA/Dex-g-OE-DOX and Dex-g-OE-DOX) with the desirable drug loading contents. In vitro cellular uptake and growth inhibition assays suggested that PBA/Dex-g-OE-DOX micelles were more efficiently internalized by monolayer tumor cells and three-dimensional multicellular tumor spheroids (MCTS) than nontargeted micelles (Dex-g-OE-DOX), leading to the fast and complete destruction of MCTS in vitro.

Introduction

Nanoscaled drug carriers are regarded as one of the most advanced and promising approaches for cancer treatment [1–3]. However, the clinical efficacy is still far from satisfaction because of the poor blood stability, nonspecific drug delivery and uncontrolled drug release [4–6]. Furthermore, the expensive raw material and complicated synthesis process also limit

the clinical application of therapeutic agents [6, 7]. Thus, it is high demand to develop facile and powerful nanocarriers with excellent blood stability and more prominent tumor-targeting ability to achieve a high efficacy in cancer treatment. To realize effective drug delivery from the injection site to the target tumor cells, the nanocarriers need to remain stable in blood circulation to avoid cleaning by reticuloendothelial system (RES), escape from the blood vessels and penetrate into tumor tissues, then adhere to

Address correspondence to E-mail: tangrp99@iccas.ac.cn

tumor cells for efficient cellular uptake, and finally accomplish rapid drug release [8, 9]. Fortunately, the stability of nanocarriers can be improved by utilizing coating materials with “stealth” property, such as dextran or PEG [10–12]. Particularly, dextran has been greatly used as protective shells, which protect therapeutic agents in the core, reduce plasma protein adsorption, extend the circulation time, and increase nanocarriers accumulation in tumor tissues by enhanced permeability and retention (EPR) effect [13–16].

Nevertheless, the stealthy protective shells also inhibit the effective uptake of nanoparticles by cancer cells. To obtain a satisfactory therapeutic effect, the desirable nanocarriers need to keep stealth in bloodstream and become sticky on tumor cells [17, 18]. The most useful strategy to enhance nanocarrier's tumor-targeting ability is to conjugate active ligands in nanocarriers, which can target the overexpressed receptors on the tumor cells' surfaces and induce receptor-mediated endocytosis [19, 20]. Many representative ligands such as folic acid, biotin, peptides, and phenylboronic acid (PBA) have been effectively decorated on the surface of nanocarriers for efficient cellular uptake [21–25]. PBA and its derivatives possess high affinity to sialic acid (SA), which is overexpressed on certain tumor cells such as hepatoma carcinoma cells [26]. And numerous studies have demonstrated that PBA-decorated carriers displayed significant higher therapeutic efficacy than nontargeting counterparts [27–30].

So far, a few tumor-targeted nanocarriers have been studied in clinical trials, but they cannot effectively distinguish between normal tissue and tumor sites, and then still induce serious side effects [7, 31]. In order to target the tumor tissues, some stimuli responsiveness such as pH, reduction, enzyme, and temperature has been widely explored to upgrade the therapeutic index [32–35]. Particularly, pH responsiveness is one of the most frequently used triggers because of the existence of pH gradient between extracellular matrix (pH 6.5–7.2) and endo/lysosomes spaces (pH 4.5–6.5) [36–38]. Currently, various pH-sensitive nanocarriers via acid-sensitive linkages including acetal, hydrazone, and β -amino esters have been developed to accelerate drug release [39–41]. Despite that much progress has been achieved, most of them cannot precisely differentiate the pH changes between tumorous matrix and normal tissues [42, 43]. A few researchers have tried to utilize ultra-pH-

sensitive carriers to reinforce cancer therapeutic efficacy via PEGylation and dePEGylation, protonation and deprotonation, or dynamic size transition methods [44–47]. Previously, our groups have developed some ultra-pH-sensitive nanocarriers via acid-labile ortho ester linkages in backbones, which performed the acid-triggered degradation upon pH 6.5–7.2, and thus showed greatly enhanced tumor targeting and inhibitory [48, 49].

Herein, we try to introduce the ortho ester linkages into PBA-grafted dextran main chains to give multifunctional ultra-pH-sensitive micelles, which can keep stealthy in blood circulation, respond to extracellular pH (6.5–7.2) for enhanced drug retention by enlarging size, interact with SA receptors on the tumor cell membrane and achieve rapid drug release at intracellular acid condition. Dextran as a hydrophilic natural polymer has been extensively used as the coating materials to improve nanocarriers stability and long blood circulation time because of its excellent water solubility, non-toxicity and biocompatibility properties [50–55]. The ortho ester monomer and tumor-targeting ligand (3-APBA) were grafted to dextran backbones to give new multifunctional ultra-pH-sensitive conjugates (PBA/Dex-g-OE) via a facile one-pot strategy. PBA/Dex-g-OE could readily self-assemble into nanoscaled micelles in neutral aqueous solution, and DOX was easily encapsulated. In vitro cellular uptake and antitumor activity of empty and DOX-loaded PBA/Dex-g-OE micelles were investigated by monolayer cell models and three-dimensional cultured multicellular tumor spheroids (MCTS).

Experimental section

Materials

Dextran (Dex, $M_w = 15000$ – 25000), N,N' -carbonyldiimidazole (CDI), Hoechst 33258 and 3-(4,5-dimethylthiazol-2-yl)-2,5-diphenyl tetrazodium bromide (MTT) were purchased from Sigma-Aldrich. 3-Aminophenylboronic acid (3-APBA, $\geq 98\%$) was obtained from Aladdin. Doxorubicin hydrochloride (DOX·HCl) was obtained from Meilun Biological Technology Co., Ltd and desalted with TEA before use. The Dulbecco's Modified Eagle's Medium (DMEM) and fetal bovine serum (FBS) were purchased from Gibco. Human liver carcinoma cell lines

(HepG2) and murine hepatic cancer cell lines (H22) were purchased from KeyGENBioTECH (Nanjing, China). Dimethyl sulfoxide (DMSO) was dried over CaH_2 and distilled under reduced pressure. The ortho ester monomer C-(2-methoxy-[1,3]dioxolan-4-yl)methylamine (indicated as OE) was synthesized as described previously [56].

Synthesis of Dex-g-OE and PBA/Dex-g-OE conjugates

Amphiphilic Dex-g-OE conjugates were synthesized by the partial modification of dextran with ortho ester monomer (OE) in the presence of CDI. The molar feed ratios of Dex/CDI/OE = 1:(1.1, 1.3, or 1.5):(1.1, 1.3, or 1.5). The exemplary feed ratio of 1:1.3:1.3 was selected to describe the synthetic procedure of Dex-g-OE in detail. Briefly, under a nitrogen atmosphere, dextran (1.62 g, 10 mmol) was dissolved in 30 mL anhydrous DMSO at 25 °C. CDI (2.11 g, 13 mmol) was added to the solution of dextran and stirred for 2 h to activate the hydroxyl groups of dextran. Then, ortho ester monomer (OE) (1.73 g, 13 mmol) in 10 mL anhydrous DMSO was dropwise added to the mixture, and the reaction solution was stirred vigorously at 25 °C for another 12 h. The resulting Dex-g-OE conjugates were isolated by precipitation from the cold diethyl ether. Then, the precipitate was collected and dialyzed (MWCO 3500 Da) against distilled water with a trace amount of triethylamine for 48 h. Finally, the sample of dialysis was lyophilized to give a white powder (3.21 g, 87% yield). The chemical structure of Dex-g-OE was analyzed by ^1H NMR in $\text{DMSO-}d_6$.

Similarly, PBA/Dex-g-OE conjugates were also fabricated with the same methods, except that 0.14 g (10 mmol) 3-APBA was co-dissolved with 1.73 g (13 mmol) OE in 10 mL DMSO. The molar feed ratio of Dex/CDI/OE/PBA = 1:1.4:1.3:0.1 was selected for subsequent experiments. And the resulting product was purified by the same process described above to obtain PBA/Dex-g-OE conjugates (3.15 g, 82% yield). The chemical structure of PBA/Dex-g-OE was also characterized by ^1H NMR in $\text{DMSO-}d_6$. The molecular weight and PDI of Dex-g-OE and PBA/Dex-g-OE conjugates were detected by Waters 1515 gel permeation chromatography (GPC) instruments in DMF at a flow rate of 1 mL/min, and a series of polystyrene standards were applied for calibration.

Preparation of Dex-g-OE and PBA/Dex-g-OE micelles

Dex-g-OE and PBA/Dex-g-OE-based micelles were prepared as follows: Dex-g-OE or PBA-Dex-g-OE conjugates (30 mg) were dissolved in DMSO (2 mL) with a trace amount of triethylamine. Under vigorously stirring, 10 mL of pH 7.4 buffer (0.01 M) was subsequently added dropwise to the polymer solution and the mixture was further stirred for 2 h. The resulting micelles were moved to a dialysis membrane (MWCO 3500 Da) and dialyzed against PBS (0.01 M, pH 7.4) for 48 h to remove solvents. The dialyzed against water was exchanged with fresh water with a trace amount of triethylamine every 3 h in 24 h. Finally, the polymeric micelles were obtained by lyophilization.

Characterization of Dex-g-OE and PBA/Dex-g-OE micelles

^1H NMR spectra were recorded on a Bruker Advance III 400 MHz Digital NMR spectrometer using deuterated dimethyl sulfoxide ($\text{DMSO-}d_6$) as the solvent. The average hydrodynamic diameter and distribution of Dex-g-OE and PBA/Dex-g-OE micelles were measured by dynamic light scattering (DLS) using Nano-ZS90 apparatus (Malvern Instruments). All samples were diluted with PBS (0.01 M, pH 7.4) to achieve a proper concentration before testing. The morphology of the micelles was observed by transmission electron microscopy (TEM) (JEM-2100, Japan). And the conjugation of 3-aminophenylboronic acid was detected by ICP-MS measurement (ICAP 7400 Duo) [30]. Elemental analysis was employed to evaluate the substitution degree of the ortho ester monomer (OE) using a Vario EL-3. The change of size and colloid status of Dex-g-OE and PBA/Dex-g-OE micelles at neutral condition (pH 7.4) were detected continuously in 10 days to verify long-time storage stability. Moreover, micelles' stability in different conditions were also performed by DLS.

Determination of the critical micelle concentration (CMC)

The critical micelle concentration (CMC) of Dex-g-OE and PBA/Dex-g-OE micelles was determined using Nile Red as a fluorescence probe [57]. Briefly, 20 μL

of Nile Red solution (1×10^{-4} mol/L) in acetone was added to a series of 10 mL brown volumetric flasks and then acetone was evaporated. Then, 2 mL of different concentrations of Dex-g-OE or PBA/Dex-g-OE micelles solutions (ranging from 1×10^{-7} to 5 mg/mL) was added into the flasks. All samples were incubated overnight at room temperature in the dark and performed using a Shimadzu Spectrofluorophotometer RF-5301PC Series with the excitation wavelength of 554 nm. The emission spectra were recorded from 550 to 720 nm. The CMC values were determined at the inflection point on the plots representing the maximum emission wavelength as a function of micelles concentration.

pH-triggered behaviors

pH-triggered degradation behaviors of Dex-g-OE and PBA-Dex-g-OE micelles were detected by ^1H NMR and DLS, respectively. Briefly, freeze-dried Dex-g-OE or PBA-Dex-g-OE micelles (10.0 mg) were dispersed in 2 mL PBS (0.01 M, pH 5.5, 6.5, and 7.4) and placed in a shaking table with a rotation speed of 120 rpm at 37 °C. At different time point, the particle size and count rate changes of micelles in response to different pHs (0.01 M, pH 5.5, 6.5, and 7.4) were monitored by DLS. Then, the solutions were lyophilized and then analyzed by ^1H NMR using DMSO- d_6 as a solvent. Otherwise, the images of PBA-Dex-g-OE micelles incubated with PBS (0.01 M, pH 6.5 and 5.5) for 9 h were captured by TEM.

Preparation of DOX-loaded micelles

The DOX-loaded micelles were fabricated by the same method with empty micelles, except that 6 mg of desalted DOX was co-dissolved with 30 mg Dex-g-OE or PBA/Dex-g-OE conjugates in 2 mL DMSO. Then, the micelles were centrifuged at 12000 rpm for 15 min, then washed and re-suspended with 4 mL PBS (0.01 M, pH 7.4). The suspension was lyophilized to obtain DOX-loaded micelles (Dex-g-OE-DOX or PBA/Dex-g-OE-DOX). To calculate the drug loading content (DLC) and drug loading efficiency (DLE), the freeze-dried DOX-loaded micelles were dissolved in DMSO, and optimal absorbance of DOX at 481 nm was recorded by microplate reader (M2^e Molecule Devices, USA). And a standard curve was prepared by using the free DOX solution at the same conditions. The drug loading content (DLC) and the drug

loading efficiency (DLE) were calculated as follows: $\text{DLC}\% = (\text{weight of the DOX in micelles})/(\text{weight of the micelles}) \times 100\%$; $\text{DLE}\% = (\text{weight of the DOX in micelles})/(\text{weight of the feeding drug}) \times 100\%$.

In vitro drug release

The release profile of DOX from DOX-loaded micelles was studied by a dialysis method. Typically, 1.0 mL Dex-g-OE-DOX or PBA/Dex-g-OE-DOX suspension with known drug concentration (0.5 mg/mL) was transferred into a dialysis bag (MWCO 14 kDa) and immersed into 20 mL PBS (0.01 M, pH 5.5, 6.5, and 7.4) solution with continuously shaken (120 rpm) at 37 °C. At preset time intervals, 1.0 mL release media was sampled and replaced with an equal volume of fresh PBS. The amount of DOX released from Dex-g-OE-DOX and PBA/Dex-g-OE-DOX was measured using a microplate reader (M2^e Molecule Devices, USA) at 481 nm. All experiments were carried out in triplicate.

In vitro cytotoxicity assay

The cytotoxicity of free DOX, blank micelles, and DOX-loaded micelles was estimated in vitro by MTT assay with H22 and HepG2 cells. Briefly, two kinds of cells were seeded in 96-well plates (5×10^3 cells/well) and cultured at 37 °C with 5% CO₂ for 24 h to allow cells attachment, respectively. The medium was replenished by 180 μL of fresh medium and 20 μL of free DOX, DOX-loaded micelles at final DOX concentration ranging from 0.5 to 16 $\mu\text{g}/\text{mL}$ or empty Dex-g-OE and PBA/Dex-g-OE micelles at final concentration ranging from 1 to 1000 $\mu\text{g}/\text{mL}$, respectively. The cells were further cultured at 37 °C in a humidified atmosphere with 5% CO₂ for 24 h. Then, the culture medium was removed and washed with PBS three times. Instead, 180 μL of fresh medium and 20 μL of MTT solution (5 mg/mL) in PBS were added to each well for another 4 h. Finally, the medium in each well was removed and 150 μL of DMSO was added to dissolve the formazan crystals. The absorbance at 570 nm of each well was recorded on a microplate reader after vibrating for 10 min in the dark.

Cellular uptake and flow cytometry

The cellular uptake of DOX-loaded micelles was assessed by confocal laser scanning microscope (CLSM) and flow cytometry against HepG2 and H22 cells. Taking HepG2 cells as an example, briefly, HepG2 cells were seeded in 6-well plate containing a cover glass and cultured for 24 h. Then, the original medium was replaced by 2 mL of fresh DMEM containing DOX-loaded micelles or free DOX with equivalent DOX concentration (8 $\mu\text{g}/\text{mL}$). After 4-h incubation, the culture medium was removed and washed with PBS (0.01 M, pH 7.4) twice. The cells were fixed with 4% paraformaldehyde, and the nuclei were dyed with Hoechst 33258 for 15 min, respectively. All samples were cleaned with PBS before imaging by CLSM. H22 cells were also evaluated as the same method.

In vitro cellular uptake of these DOX-loaded micelles was further quantified by flow cytometry. HepG2 and H22 cells were placed into 6-well plate at a concentration of 1×10^5 cells/well and allowed to adhere for 24 h. Next, free DOX, Dex-g-OE-DOX, and PBA/Dex-g-OE-DOX were added to each well with a final drug dosage of 8 $\mu\text{g}/\text{mL}$ for 4 h. The culture medium was removed, and the cells were washed with PBS three times. Finally, all cell samples were collected by centrifugal and dispersed into 0.8 mL of PBS, and the fluorescence intensity of DOX in each sample was investigated using a BD flow cytometry.

Formation of HepG2 multicellular tumor spheroids (MCTS)

The MCTS of HepG2 cells were built as previously reported [58, 59]. Briefly, a layer of poly(2-hydroxyethyl methacrylate) (PHEMA) thin film was coated on the bottom of cell culture flasks to avoid adhering. Then, HepG2 cells (5×10^5) in 5 mL of fresh medium were added into a PHEMA-coated cell culture flask. The cells were cultured under the humidified atmosphere with 5% CO_2 at 37 $^\circ\text{C}$, and the medium was replaced by fresh medium every 2 days. The MCTS were formed with the size about 200–300 μm in a week.

The penetration and growth inhibition study in HepG2 MCTS

After several days of growth, MCTS with the diameter about 220 μm were gathered and co-cultured with free DOX and DOX-loaded micelles (final dosage of 8 $\mu\text{g}/\text{mL}$), respectively. At different time intervals (2, 4, 8, 12, and 24 h), the MCTS were thoroughly washed with PBS and then imaged by CLSM. In addition, the fluorescence intensity of DOX in each MCTS was estimated by using Image J. Z-stack. The cytotoxicities of free DOX, empty micelles and DOX-loaded micelles against MCTS were determined by a growth inhibition assay. MCTS with a diameter about 220 μm were collected and co-incubated with empty micelles, free DOX, and DOX-loaded micelles (final dosage 8 $\mu\text{g}/\text{mL}$) for 5 days at 37 $^\circ\text{C}$, respectively. The diameter of each spheroid was measured every other day after images were recoded by optical microscope.

Results and discussion

Synthesis of Dex-g-OE and PBA-Dex-g-OE

Dex-g-OE conjugates were prepared by grafting ortho ester monomer (OE) to the backbones of dextran using CDI as an activator (Scheme 1a). The chemical structure of Dex-g-OE was verified by ^1H NMR spectra (Fig. 1a). The characteristic chemical shift at 5.75–5.77 ppm belonged to the special shift of ortho ester proton, and other proton signals corresponded well to their molecular structures. Similarly, PBA/Dex-g-OE conjugates were also readily obtained by grafting ortho ester monomer (OE) and tumor-targeting ligand (3-APBA) to dextran through their terminal amine groups, as shown in Scheme 1b. ^1H NMR (Fig. 1b) spectra confirmed PBA/Dex-g-OE was structurally correct. The peaks at δ (ppm) 5.75–5.77 belonged to the special shift of ortho ester proton, and other new peaks arising at 6.54, 6.89–6.93, and 7.59 ppm correspond to the phenyl protons of PBA. The average molecular weights of Dex, Dex-g-OE, and PBA/Dex-g-OE were measured by GPC to be 1.69, 1.87, and 2.05×10^4 with PDI of 1.37, 1.54, and 1.45, respectively (Table S1, Supporting Information), which indicated that the dextran did not conjugate with each other, and Dex-g-OE and PBA/Dex-g-OE conjugates were successfully prepared.

Scheme 1 Synthesis route of Dex-g-OE (a) and PBA/Dex-g-OE (b) conjugates. Reaction conditions: (i) N,N'-Carbonyldiimidazole (CDI); (ii) DMSO.

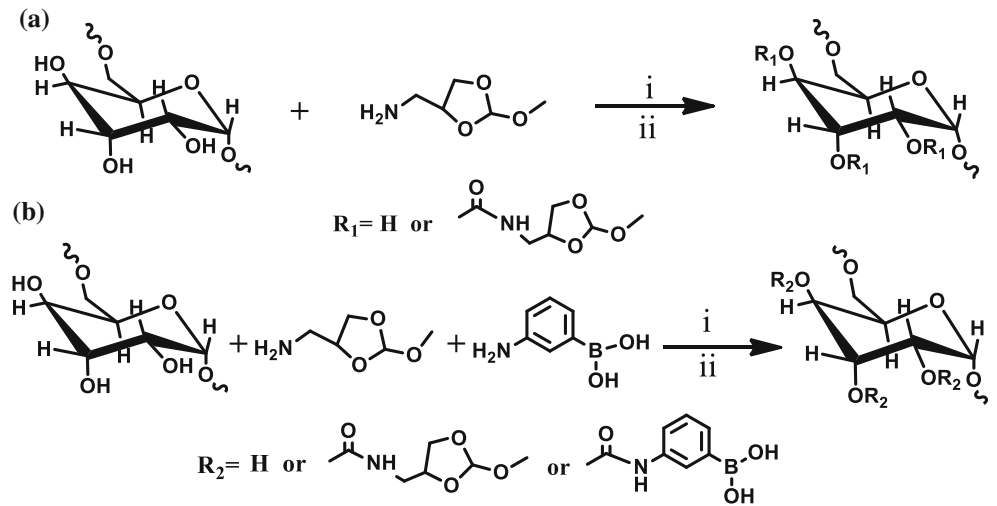
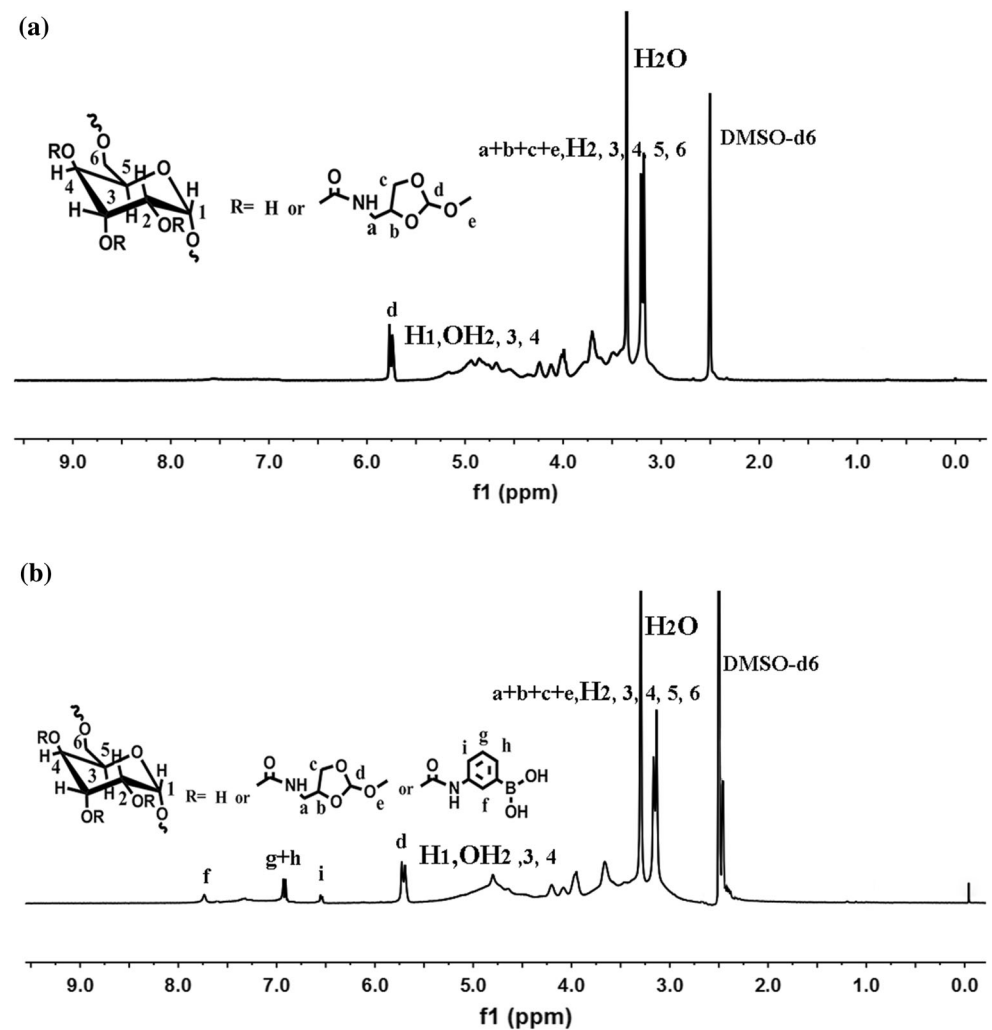


Figure 1 ^1H NMR spectra of Dex-g-OE (a) and PBA/Dex-g-OE (b) in $\text{DMSO-}d_6$.



Fabrication and characterization of micelles

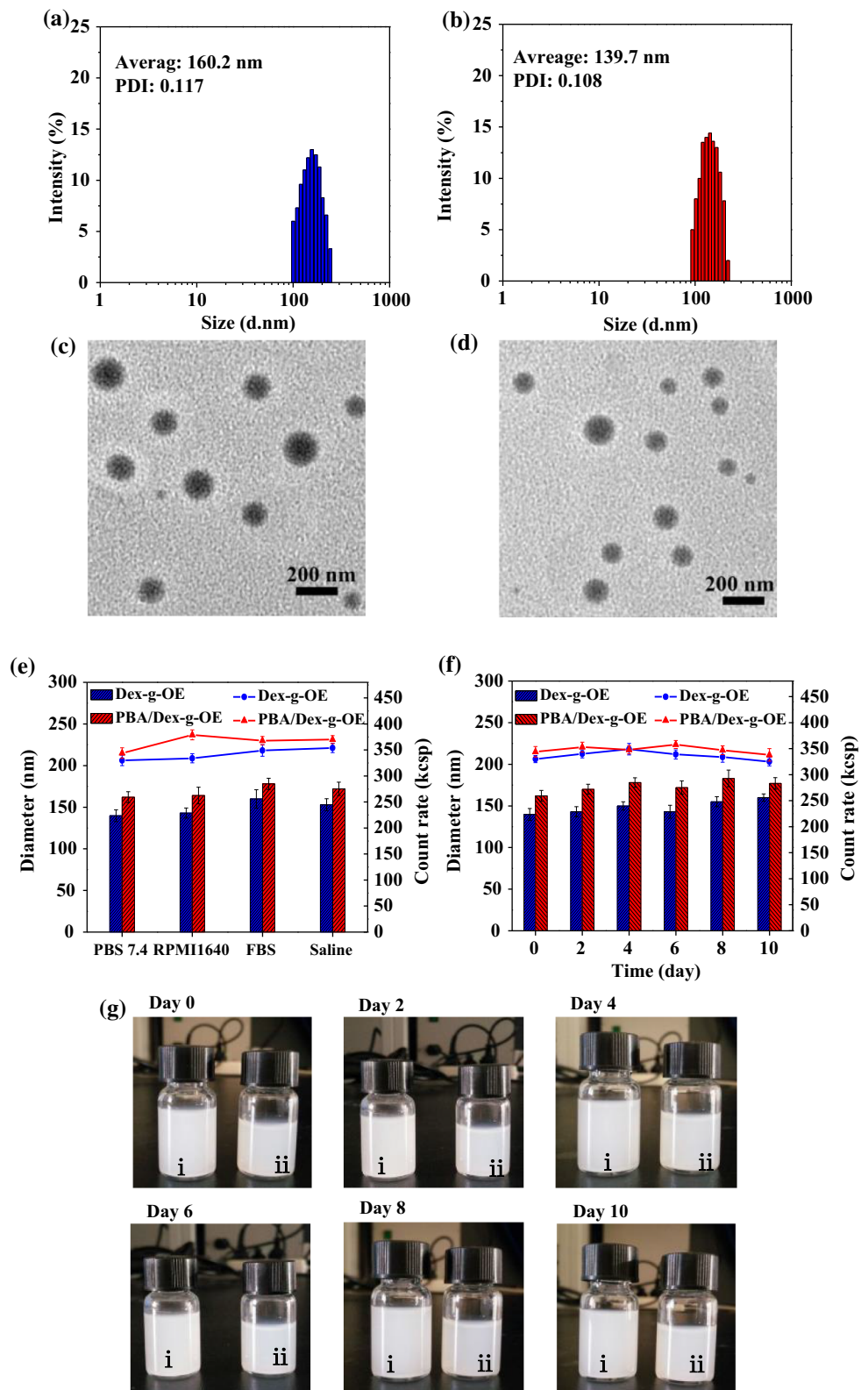
Dex-g-OE and PBA/Dex-g-OE as amphipathic copolymers could easily self-assemble into nanoscaled micelles in neutral aqueous solution. The size of Dex-g-OE micelles could be controlled by regulating the molar feed ratio of Dex to OE. The diameter of Dex-g-OE micelles with different feed ratio was detected by DLS, as given in Table S2. The size of Dex-g-OE micelles varied from 139.7 to 268.9 nm, which should be suitable for drug delivery and accumulation into tumor tissues. So, the feed ratio of Dex to OE (1/1.3) was chosen to prepare Dex-g-OE and PBA/Dex-g-OE micelles. As shown in Fig. 2a, b, the diameter of Dex-g-OE and PBA/Dex-g-OE micelles was less than 170 nm with a narrow size distribution ($PDI < 0.15$), which was appropriate for tumor targeting by the EPR effect. TEM images (Fig. 2c, d) indicated that Dex-g-OE and PBA/Dex-g-OE micelles had a uniform spherical shape and the size was smaller than that was determined by DLS, which were probably attributed to the dehydration effect of micelles in TEM preparation. The zeta potential of Dex-g-OE and PBA/Dex-g-OE micelles was -6.4 mV and -4.3 mV, which will be good for blood circulation and decreasing interactions with biomolecules present in the blood. The critical micelle concentration (CMC) measurements using Nile Red as a fluorescence probe showed that Dex-g-OE and PBA/Dex-g-OE micelles have low CMC values of 2.3×10^{-4} and 7.6×10^{-4} mg/mL (Figure S1), indicating that these micelles could keep stable during the blood circulation. The kinetic stability of Dex-g-OE and PBA/Dex-g-OE micelles in PBS 7.4 was evaluated by DLS. As shown in Fig. 2f, g, the change of size and colloid status for both micelles were negligible in 10 days, suggesting that these micelles could perform desirable long-term stability. Furthermore, Dex-g-OE and PBA/Dex-g-OE micelles also exhibited high stability in different physiological conditions (Fig. 2e). The grafting degree of ortho ester was measured by the elemental analysis (Table 1). Moreover, the PBA graft value of PBA/Dex-g-OE was calculated to be 9.7% by ICP-MS measurement (Table 1).

Ultra-pH sensitivity of Dex-g-OE and PBA/Dex-g-OE

In order to validate the ultra-pH sensitivity of Dex-g-OE and PBA/Dex-g-OE conjugates, the degradation kinetic of ortho ester in micelles was performed at different pH conditions (pH 5.5, 6.5, and 7.4), and then the samples were lyophilized and analyzed by ^1H NMR. As expected, the hydrolysis of ortho esters at pH 7.4 was paltry for 72 h, but was much accelerated at slightly acidic conditions (pH 5.5 and 6.5). Briefly, ortho ester bonds of Dex-g-OE and PBA/Dex-g-OE micelles were completely hydrolyzed in 7.5 h and 9 h at pH 5.5, respectively. And the hydrolysis of ortho esters in Dex-g-OE and PBA/Dex-g-OE micelles was complete in 20 h and 24 h at pH 6.5 (Figs. 3, 4a). These results indicated that Dex-g-OE and PBA/Dex-g-OE micelles showed the ultra-pH sensitivity, which could be sensitive to the tumor extracellular (pH 6.5–7.0) and intracellular environments (pH 5.5–6.5). Moreover, the characteristic proton peak of ortho ester at δ 5.77 ppm reduced gradually at pH 5.5 and 6.5, and a new proton peak of formate at δ 8.23 ppm emerged and the peak intensity increased with the extend of treated time. In addition, the hydrolysis of cyclic ortho ester in Dex-g-OE and PBA/Dex-g-OE also followed an exocyclic pathway, which was the same with previously reported studies (Scheme S1) [60–62].

The size and count rate change of two micelles in response to different pH values were also detected by DLS. As revealed in Fig. 4b, c, the diameter of two micelles was hardly changed over 24 h at pH 7.4, which was probably due to the slow hydrolysis rate of ortho esters (Fig. 3). On the contrast, the average size of Dex-g-OE and PBA/Dex-g-OE micelles increased to 458 and 481 nm in initial 6 h at pH 5.5, respectively. Surprisingly, the diameter of two micelles almost disappeared at pH 5.5 after incubating for 9 h, which revealed that the acid-triggered rapid hydrolysis of ortho esters could induce the swelling and dissolution or agglomeration of micelles. The diameter of micelles gradually increased from 143 to 311 nm (Dex-g-OE) and from 161 to 371 nm (PBA/Dex-g-OE) in 12 h and then decreased to 46 nm (Dex-g-OE) and 90 nm (PBA/Dex-g-OE) at pH 6.5 after treated for 24 h, respectively. This result was probably because of the slow hydrolysis of ortho esters at pH 6.5, which might be conducive to drug retention in deeper tumor areas

Figure 2 Size distribution of PBA/Dex-g-OE (a) and Dex-g-OE (b) micelles by DLS; TEM images of PBA/Dex-g-OE (c) and Dex-g-OE (d) micelles, scale bar 200 nm; the stability of PBA/Dex-g-OE and Dex-g-OE micelles in different physiological conditions (e); time-dependent stability of PBA/Dex-g-OE and Dex-g-OE micelles in PBS (pH 7.4) for 10 days (f); the long-time storage stability of Dex-g-OE (i) and PBA/Dex-g-OE (ii) micelles in PBS (pH 7.4) for 10 days (g).



after the micelles accumulated at the tumor extracellular microenvironments [49, 63]. Furthermore, we also found that the count rate of micelles at mildly

acidic conditions continuously declines, while only slight change was observed at pH 7.4 (Fig. 4d). As shown in Figure S2a and 2b, TEM images of PBA/

Table 1 Characterization of micelles formulations

Formulation	Size ^a (nm)	PDI ^a	Zeta ^b (mV)	Graft ratio of OE ^c (%)	Graft ratio of PBA ^d (%)
Dex-g-OE	139.7 ± 10.8	0.112 ± 0.006	− 6.4 ± 0.6	20.8	–
PBA/Dex-g-OE	160.2 ± 14.3	0.117 ± 0.015	− 4.3 ± 1.2	19.6	9.7

Data are reported as mean ± SD ($n = 3$)

^aDetermined by DLS in PBS buffer (0.01 M, pH 7.4)

^bDetermined by zeta potential accessory attached to DLS in PBS buffer (0.01 M, pH 7.4)

^cDetermined by elemental analysis

^dDetermined by ICP-MS

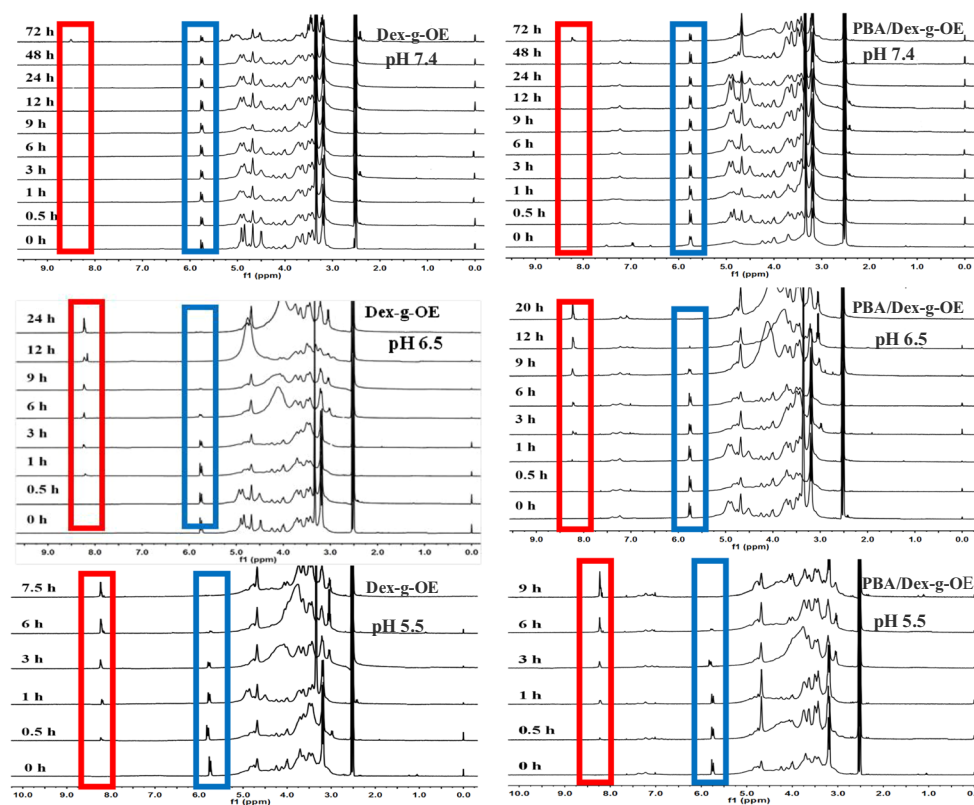


Figure 3 ^1H NMR spectra of Dex-g-OE and PBA/Dex-g-OE at different pHs; peaks indicated in red and blue rectangles represent characteristic protons of ortho ester and formate, respectively.

Dex-g-OE micelles (incubated at pH 6.5 and 5.5 for 9 h, respectively) showed that the size of micelles continued to increase at pH 6.5, while the micelles almost lost their micromorphology structure at pH 5.5. These results also demonstrated that PBA/Dex-g-OE was ultra-pH sensitive, which could respond to the extracellular pH (6.5–7.2) for enhanced drug retention by enlarging size and achieve rapid drug

release at the intracellular acid condition (pH 5.5–6.5).

DOX loading and in vitro drug release

In this study, DOX was easily loaded into the core of micelles to give Dex-g-OE-DOX and PBA/Dex-g-OE-DOX. As given in Table 2, DLC of Dex-g-OE-DOX and PBA/Dex-g-OE-DOX was 11.8% and 17.1%, respectively, which corresponded to DLE of 78.5%

Figure 4 Hydrolysis kinetics of Dex-g-OE and PBA/Dex-g-OE micelles at pH 7.4, 6.5, and 5.5 (a); time and pH-dependent changes of average size of Dex-g-OE (b) and PBA/Dex-g-OE (c) micelles in different aqueous phosphate buffer (pH 7.4, 6.5, and 5.5) measured by DLS; the count rate change of Dex-g-OE and PBA/Dex-g-OE micelles (d) in different pHs (7.4, 6.5, and 5.5).

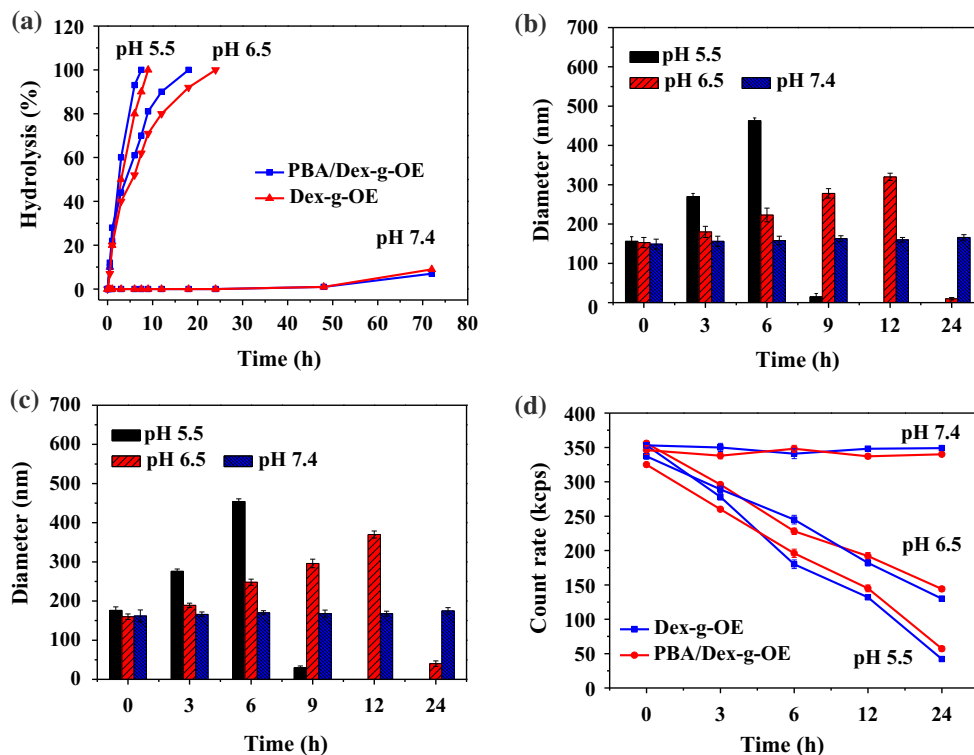


Table 2 Characterization of DOX-loaded micelle formulations

Formulation	Size ^a (nm)	PDI ^a	DLC ^b (%)	DLE ^b (%)
Dex-g-OE-DOX	171.0 ± 11.2	0.163 ± 0.016	11.8 ± 0.7	78.5 ± 4.2
PBA/Dex-g-OE-DOX	186.4 ± 16.1	0.125 ± 0.037	17.1 ± 1.1	88.7 ± 6.9

^aDetermined by DLS in PBS (0.01 M, pH 7.4)

^bDetermined by spectra Max M2^e Molecular devices at 481 nm.; data are represented as mean ± SD ($n = 3$)

and 88.7%. The DOX-loaded micelles were 30 nm larger than the blank micelles with a desirable PDI in aqueous medium.

In order to study the influence of pH on the drug release of DOX-loaded micelles, *in vitro* drug release profiles were monitored at different pH values (PBS, pH 5.5, 6.5, and 7.4). As shown in Fig. 5a, less than 15% of DOX was released in 48 h at neutral environment (pH 7.4). Obviously, drug release in neutral environment was strictly suppressed due to the coordination effect between DOX and ortho esters, as well as the high stability of micelles, while the DOX release rate was remarkably accelerated at mildly acidic conditions, and the cumulative DOX release attained 91% (PBA/Dex-g-OE-DOX) and 88% (Dex-g-OE-DOX) within 24 h at pH 5.5, respectively. At pH 6.5, the DOX release showed a similar trend, which attained 62% (Dex-g-OE-DOX) and 66% (PBA/Dex-g-

OE-DOX) in 36 h, respectively. Otherwise, there was no significant difference in the drug release between PBA/Dex-g-OE-DOX and Dex-g-OE-DOX at tested pH values, indicating that the 3-APBA-modified micelles had no obvious effect on drug release. Thus, these ultra-pH-sensitive micelles possessed great potential to kill tumor cells, which may minimize the off-target toxicity and provide a sufficient amount of agents in cancer therapy.

In vitro cytotoxicity assay

The cytotoxicity of empty and DOX-loaded micelles was verified by MTT assay on H22 and HepG2 cell lines for 24 h. As shown in Fig. 5b, the viability of Dex-g-OE and PBA/Dex-g-OE micelles was over 93% even at high treated concentration of 1 mg/mL, indicating Dex-g-OE and PBA/Dex-g-OE micelles

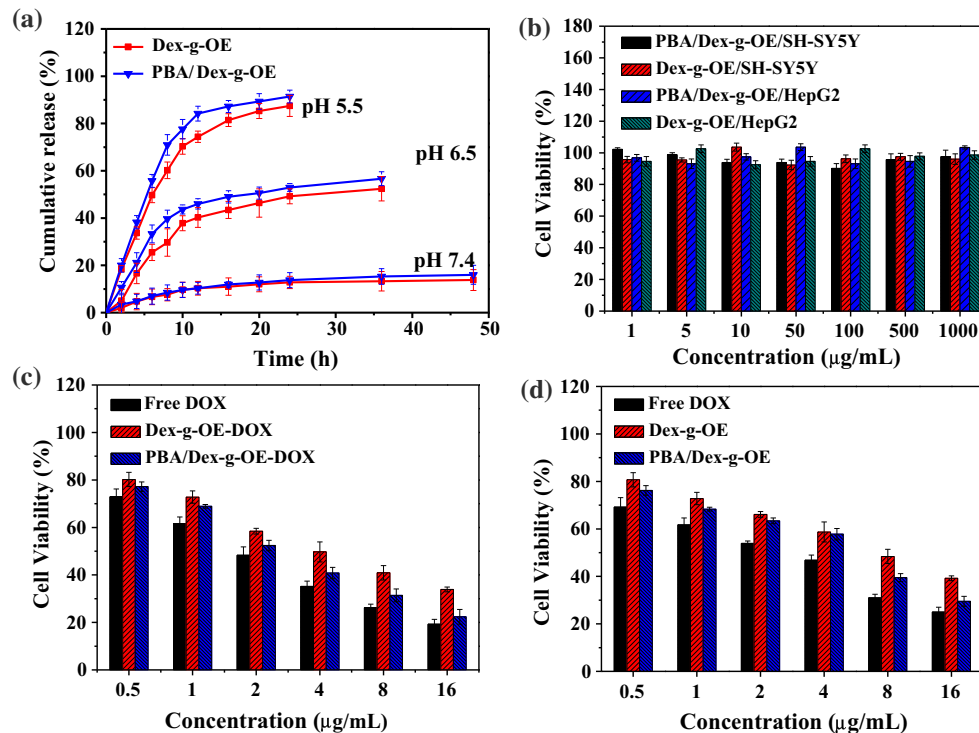


Figure 5 Release kinetics of the loaded DOX in Dex-g-OE and PBA/Dex-g-OE micelles at pH 7.4, 6.5, and 5.5 (a); in vitro cytotoxicity of Dex-g-OE and PBA/Dex-g-OE micelles co-cultured with H22 and HepG2 cells for 24 h (b); dose-

dependent cytotoxicity of free DOX, Dex-g-OE-DOX, and PBA/Dex-g-OE-DOX on HepG2 (c) and H22 (d) cells for 24 h in vitro determined by MTT assay.

had excellent biocompatibility. On the contrary, a dose-dependent decrease in cell viability was displayed in two cells after incubation with free DOX and DOX-loaded micelles (Fig. 5c, d). Dex-g-OE-DOX and PBA/Dex-g-OE-DOX micelles showed lower cytotoxicity than free DOX at all tested concentrations, which might be attributed to the sustained DOX release. It should be noted that PBA/Dex-g-OE-DOX micelles showed lower cell viability than Dex-g-OE-DOX at corresponding concentrations against two cell lines. For PBA/Dex-g-OE-DOX, the viability declined to 27% (H22) and 22% (HepG2) at higher DOX concentration of 16 µg/mL, respectively. As for Dex-g-OE-DOX, the viability of H22 cells and HepG2 cells decreased to 35% and 33% at the same conditions (16 µg/mL), respectively. The IC₅₀ (Figure S3) values of PBA/Dex-g-OE-DOX micelles were lower than that of Dex-g-OE-DOX micelles against H22 and HepG2 cells, which was probably caused by the higher ligand–receptor interactions between SA receptors and PBA derivatives.

Cellular uptake and intracellular drug release

In order to assess cellular uptake and drug delivery in tumor cells, free DOX and DOX-loaded micelles were co-cultured with H22 and HepG2 cells for 4 h, respectively, and then the cells were imaged by CLSM. After 4 h incubation, a weak red signal of DOX was observed in cell nuclei for free DOX-treated cells. Compared to free DOX, DOX-loaded micelles possessed a higher intensity of DOX fluorescence signal in cells cytoplasm and nuclei (Fig. 6a, b), indicating that Dex-g-OE-DOX and PBA/Dex-g-OE-DOX micelles could be quickly internalized into tumor cells and effectively release drug in cytoplasm. Importantly, PBA/Dex-g-OE-DOX-treated cells showed much stronger DOX fluorescence than Dex-g-OE-DOX both in the cytoplasm and the nuclei, suggesting that more PBA/Dex-g-OE-DOX micelles were internalized into cancer cells than Dex-g-OE-DOX.

To further study the cellular uptake and drug delivery in tumor cells, flow cytometry was used to

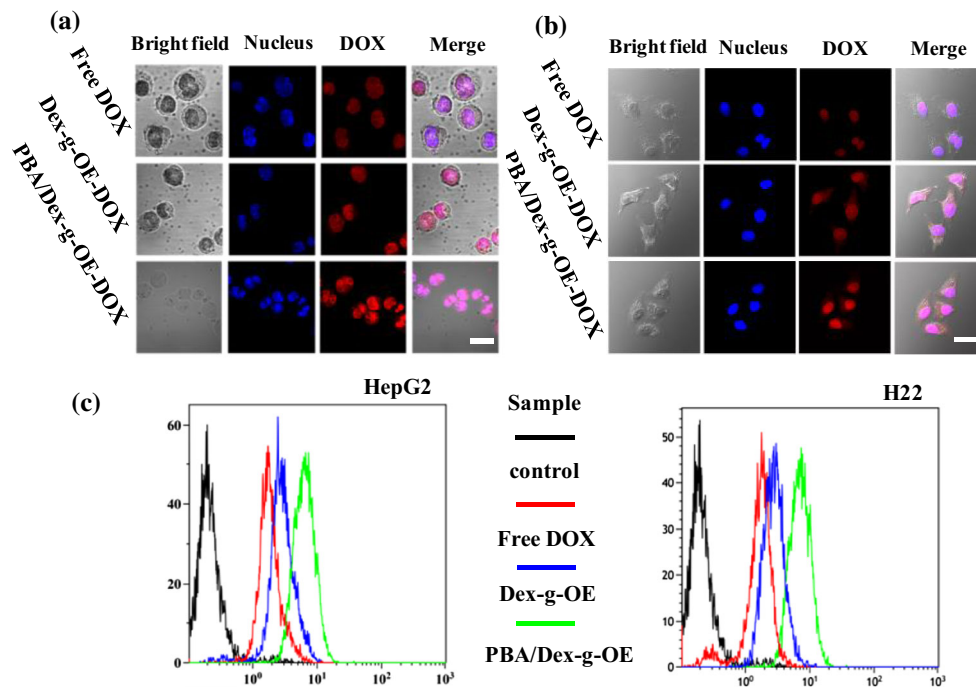


Figure 6 Representative images of H22 (a) and HepG2 (b) cells co-incubated with all tested DOX formulations by CLSM, scale bar 10 μ m; cellular uptake of control, free DOX, Dex-g-OE-DOX, and PBA/Dex-g-OE-DOX determined by flow cytometry (c).

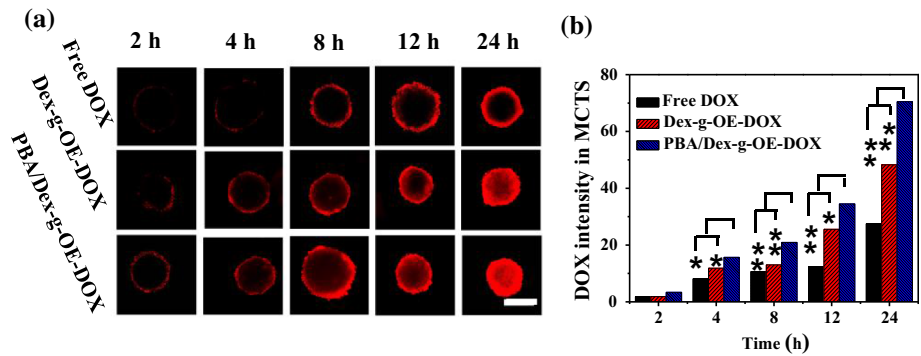
offer quantitative analysis. H22 and HepG2 cells were selected and incubated with free DOX and DOX-loaded micelles for 4 h. As shown in Fig. 6c, the DOX fluorescence intensity of PBA/Dex-g-OE-DOX micelles was higher than Dex-g-OE-DOX and free DOX in each cell line, which was consistent with the results of CLSM as described above. Moreover, the cell uptake efficiency of DOX-loaded micelles against HepG2 and H22 cells was quantitatively measured by testing the DOX fluorescence intensity for 4 h. Figure S4a shows that the DOX fluorescence intensity in HepG2 and H22 cell lines increased in the following order: free DOX, Dex-g-OE-DOX, and PBA/Dex-g-OE-DOX. Notably, the DOX fluorescence intensity was 3.54-fold (HepG2) and 3.67-fold (H22) higher than that of free DOX at 4 h (Figure S4b). All results demonstrated that the functionalized PBA/Dex-g-OE-DOX micelles could be more efficiently internalized into SA-positive tumor cells via receptor-mediated endocytosis.

Penetration and growth inhibition on HepG2 cells MCTS

To further investigate antitumor efficacy of DOX-loaded micelles, the multicellular spheroids (MCTS)

were selected to evaluate the penetration and accumulation effect of drug delivery system [64]. Free DOX and DOX-loaded micelles were incubated with HepG2 MCTS for 2, 4, 8, 12, and 24 h, respectively. The representative images of MCTS were imaged by CLSM (Fig. 7a). Clearly, a time-dependent penetration and accumulation behavior could be observed in all tested samples, and the DOX fluorescence intensity increased with the extension of treatment time. The penetration of free DOX into MCTS was tightly limited to the outer regions of the spheroids even treated for 24 h, while the weak red fluorescence of DOX-loaded micelles diffused deeper into the center of the MCTS at initial 4 h and gradually occupied the entire MCTS after 24 h co-incubation. This result demonstrated that DOX-loaded micelles could efficiently penetrate deeper into the interior of spheroids than free DOX, which was probably because the positively charged DOX-loaded micelles were avidly binding with negatively charged cell membranes and tightly limited by extracellular matrix [49, 65]. Otherwise, DOX-loaded micelles could achieve dynamic size change in response to extracellular acidic condition (pH 6.5), which could facilitate drugs diffuse into the tumor matrix and then be retained due to micelles swelling. Figure 7b shows the

Figure 7 CLSM images of HepG2 MCTS incubated with free DOX, Dex-g-OE-DOX, or PBA/Dex-g-OE-DOX for 2, 4, 8, 12, and 24 h (a), respectively, scale bar 200 μm; fluorescence intensity of MCTS at different time points (b), * represents $p < 0.05$, ** represents $p < 0.01$.

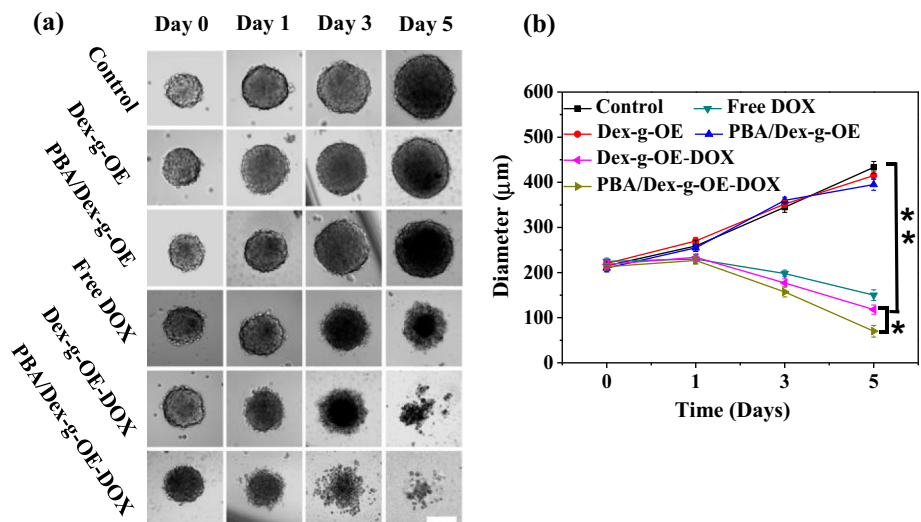


semiquantitative analysis of DOX fluorescence in each drug-treated HepG2 MCTS, and the results were in agreement with the above described. It was worth highlighting that the highest red signal and deepest penetration was observed from the PBA/Dex-g-OE-DOX-treated MCTS at each time point, indicating that the introduction of PBA could greatly improve the penetration and accumulation of micelles resulted from the receptor-mediated endocytosis.

The HepG2 MCTS with the diameter about 200–300 μm were further incubated with empty micelles, free DOX and DOX-loaded micelles for 5 days. The morphology of MCTS was imaged by the optical microscope every other day. As shown in Fig. 8a, the MCTS treated with medium (control) or empty micelles displayed a dramatic increase both in size and in volume because of the quick proliferation of cells in MCTS, which further demonstrated that

empty micelles were nontoxic and possessed excellent biocompatibility. On the contrary, the cells treated with free DOX and DOX-loaded micelles exhibited a continuous inhibition on spheroid growth, and the diameter of MCTS decreased at different extent during the 5 days, suggesting that outer layer cells of MCTS were killed. Figure 8b shows the alteration of average MCTS diameter ($n = 6$) of all tested groups during the experiment. The diameter of MCTS treated with control groups, Dex-g-OE, and PBA/Dex-g-OE increased apparently and attained to 371.2, 361.5, and 359.7 μm at day 5, respectively. By contrast, the diameter of MCTS treated with free DOX, Dex-g-OE-DOX, and PBA/Dex-g-OE-DOX micelles showed a persistent decline from 225.0 to 160.7 μm, 218.7 to 133.6 μm, and 203.2 to 90 μm, respectively. Particularly, PBA/Dex-g-OE-DOX-treated MCTS almost lost their compact 3D structure

Figure 8 Typical images of HepG2 MCTS treated with DMEM medium (control), empty micelles, free DOX, or DOX-loaded micelles (a); MCTS diameter changes after various treatments (b); scale bar 200 μm. * $p < 0.05$; ** $p < 0.01$.



after 5-day treatment, leading to the most obvious growth inhibition. These results suggested that PBA/Dex-g-OE-DOX and Dex-g-OE-DOX micelles could penetrate into MCTS and rapidly release DOX to kill tumor cells. More importantly, 3-APBA-functionalized micelles (PBA/Dex-g-OE-DOX) could more effectively penetrate into MCTS than nontargeting micelles because of the receptor-mediated endocytosis.

Conclusion

In this work, dextran acted as a stabilizing and surface-modifying agent for the synthesis of tumor-targeted ultra-pH-responsive conjugates (PBA/Dex-g-OE) and nontargeted conjugates (Dex-g-OE). Both PBA/Dex-g-OE and Dex-g-OE conjugates could easily self-assemble into stable micelles with low CMC values in neutral aqueous solution, and DOX was efficiently loaded. The PBA/Dex-g-OE micelles possessed high stability in physiological condition and were pH sensitive to both extracellular and intracellular acidic conditions, which could probably realize prolonged blood circulation, improve drug retention by increased size at pH 6.5, enhance cellular uptake via receptor-induced endocytosis, and accelerate drug release under intracellular acid conditions. In vitro MTT and cellular uptake assays revealed that the DOX-loaded micelles (PBA/Dex-g-OE-DOX) could be more effectively internalized through the receptor-mediated endocytosis and possess higher toxicity effect on tumor cells than Dex-g-OE-DOX. Moreover, in vitro penetration and growth inhibition studies also demonstrated that PBA/Dex-g-OE-DOX micelles could greatly enhance penetration and accumulation of DOX into the deeper region of MCTS, resulting in more effective growth inhibition than Dex-g-OE-DOX micelles and free DOX. All the results suggested that these tumor-targeting and ultra-pH-sensitive PBA/Dex-g-OE micelles have great potentials as drug carriers in cancer treatment.

Acknowledgements

This work is financially supported by the National Natural Science Foundation of China (Nos. 21174054, 21004030, and 51503001), the Natural Science Foundation of Anhui Province of China (No.

1408085MB26), and the Doctor Research Foundation of Anhui University of China (No. J10113190075), and the Academic and Technology Introduction Project of Anhui University of China (AU02303203), and the Nature Science Research Programme of the Education Office of Anhui Province (Nos. KJ2016A030 and KJ2018ZD003).

Compliance with ethical standards

Conflict of interest The authors have declared that there is no conflict of interest.

Electronic supplementary material: The online version of this article (<https://doi.org/10.1007/s10853-018-3092-8>) contains supplementary material, which is available to authorized users.

References

- [1] Kapri S, Maiti S, Bhattacharyya S (2016) Lemon grass derived porous carbon nanospheres functionalized for controlled and targeted drug delivery. *Carbon* 100:223–235
- [2] Rafi AA, Mahkam M, Davaran S, Hamishehkar H (2016) A smart pH-responsive nano-carrier as a drug delivery system: a hybrid system comprised of mesoporous nanosilica MCM-41 (as a nano-container) and a pH-sensitive polymer (as smart reversible gatekeepers)—preparation, characterization and in vitro release studies of an anti-cancer drug. *Eur J Pharm Sci* 93:64–73
- [3] Chen Y, Huang J, Zhang S, Gu Z (2017) Superamphiphile based cross-linked small-molecule micelles for pH-triggered release of anticancer drugs. *Chem Mater* 29:3083–3091
- [4] Bae YH, Yin HQ (2008) Stability issues of polymeric micelles. *J Control Release* 131:2–4
- [5] Liu M, Du H, Zhang W, Zhai G (2017) Internal stimuli-responsive nanocarriers for drug delivery: design strategies and applications. *Mater Sci Eng C* 71:1267–1280
- [6] Wicki A, Witzigmann D, Balasubramanian V, Huwyler J (2015) Nanomedicine in cancer therapy: challenges, opportunities, and clinical applications. *J Control Release* 200:138–157
- [7] Desai N (2012) Challenges in development of nanoparticle-based therapeutics. *AAPS J* 14:282–295
- [8] Wu Y, Chen W, Meng F, Wang Z, Cheng R, Deng C, Liu H, Zhong Z (2012) Core-crosslinked pH-sensitive degradable micelles: a promising approach to resolve the extracellular stability versus intracellular drug release dilemma. *J Control Release* 164:338–345

- [9] Xu X, Ho W, Zhang X, Bertrand N, Farokhzad O (2015) Cancer nanomedicine: from targeted delivery to combination therapy. *Trends Mol Med* 21:223–232
- [10] Massia SP, Stark J, Letbetter DS (2000) Surface-immobilized dextran limits cell adhesion and spreading. *Biomaterials* 21:2253–2261
- [11] Owen SC, Chan DPY, Shoichet MS (2012) Polymeric micelle stability. *Nano Today* 7:53–65
- [12] Deng W, Li J, Yao P, He F, Huang C (2010) Green preparation process, characterization and antitumor effects of doxorubicin–BSA–dextran nanoparticles. *Macromol Biosci* 10:1224–1234
- [13] Sun H, Guo B, Li X, Cheng R, Meng F, Liu H, Zhong Z (2010) Shell-sheddable micelles based on dextran–SS–poly(ϵ -caprolactone) diblock copolymer for efficient intracellular release of doxorubicin. *Biomacromolecules* 11:848–854
- [14] Lemarchand C, Gref R, Couvreur P (2004) Polysaccharide-decorated nanoparticles. *Eur J Pharm Biopharm* 58:327–341
- [15] Founi ME, Soliman SMA, Vanderesse R, Acherar S, Guedon E, Chevalot I, Babin J, Six JL (2018) Light-sensitive dextran-covered PNBA nanoparticles as triggered drug delivery systems: formulation, characteristics and cytotoxicity. *J Colloid Interface Sci* 514:289–298
- [16] Laville M, Babin J, Londono I, Legros M, Nouvel C, Durand A, Vanderesse R, Leonard M, Six JL (2013) Polysaccharide-covered nanoparticles with improved shell stability using click-chemistry strategies. *Carbohydr Polym* 93:537–546
- [17] Deng C, Jiang Y, Cheng R, Meng F, Zhong Z (2012) Biodegradable polymeric micelles for targeted and controlled anticancer drug delivery: promises, progress and prospects. *Nano Today* 7:467–480
- [18] Petros RA, DeSimone JM (2010) Strategies in the design of nanoparticles for therapeutic applications. *Nat Rev Drug Discov* 9:615–627
- [19] Ma X, Shi X, Bai S, Gao YE, Hou M, Han MY, Xu Z (2018) Acid-activatable doxorubicin prodrug micelles with folate-targeted and ultra-high drug loading features for efficient antitumor drug delivery. *J Mater Sci* 53:892–907. <https://doi.org/10.1007/s10853-017-1546-z>
- [20] Zha Q, Wang X, Cheng X, Fu S, Yang G, Yao W, Tang R (2017) Acid-degradable carboxymethyl chitosan nanogels via an ortho ester linkage mediated improved penetration and growth inhibition of 3-D tumor spheroids in vitro. *Mater Sci Eng C* 78:246–257
- [21] Zhang L, Wang Y, Zhang X, Wei X, Xiong X, Zhou S (2017) Enzyme and redox dual-triggered intracellular release from actively targeted polymeric micelles. *ACS Appl Mater Interfaces* 9:3388–3399
- [22] Thomas TP, Huang B, Choi SK, Silpe JE, Kotlyar A, Desai AM, Zong H, Gam J, Joice M, Baker JR (2012) Polyvalent dendrimer-methotrexate as a folate receptor-targeted cancer therapeutic. *Mol Pharmaceutics* 9:2669–2676
- [23] Heo DN, Yang DH, Moon HJ, Lee JB, Bae MS, Lee SC, Lee WJ, Sun IC, Kwon IK (2012) Gold nanoparticles surface-functionalized with paclitaxel drug and biotin receptor as theranostic agents for cancer therapy. *Biomaterials* 33:856–866
- [24] Fan X, Zhang W, Hu Z, Li Z (2017) Facile synthesis of RGD-conjugated unimolecular micelles based on a polyester dendrimer for targeting drug delivery. *J Mater Chem B* 5:1062–1072
- [25] Wang B, Chen L, Sun Y, Zhu Y, Sun Z, An T, Li Y, Lin Y, Fan D, Wang Q (2015) Development of phenylboronic acid-functionalized nanoparticles for emodin delivery. *J Mater Chem B* 3:3840–3847
- [26] Deshayes S, Cabral H, Ishii T, Miura Y, Kobayashi S, Yamashita T, Matsumoto A, Miyahara Y, Nishiyama N, Kataoka K (2013) Phenylboronic acid-installed polymeric micelles for targeting sialylated epitopes in solid tumors. *J Am Chem Soc* 135:15501–15507
- [27] Zhao Z, Yao X, Zhang Z, Chen L, He C, Chen X (2014) Boronic acid shell-crosslinked dextran-b-PLA micelles for acid-responsive drug delivery. *Macromol Biosci* 14:1609–1618
- [28] Ellis GA, Palte MJ, Raines RT (2012) Boronate-mediated biologic delivery. *J Am Chem Soc* 134:3631–3634
- [29] Ma R, Shi L (2014) Phenylboronic acid-based glucose-responsive polymeric nanoparticles: synthesis and applications in drug delivery. *Polym Chem* 5:1503–1518
- [30] Wu D, Yang J, Xing Z, Han H, Wang T, Zhang A, Yang Y, Li Q (2016) Phenylboronic acid-functionalized polyamidoamine-mediated Bcl-2 siRNA delivery for inhibiting the cell proliferation. *Colloid Interface Sci B* 146:318–325
- [31] Li J, Huo M, Wang J, Zhou J, Mohammad JM, Zhang Y, Zhu Q, Waddad AY, Zhang Q (2012) Redox-sensitive micelles self-assembled from amphiphilic hyaluronic acid–deoxycholic acid conjugates for targeted intracellular delivery of paclitaxel. *Biomaterials* 33:2310–2320
- [32] Pramod PS, Shah R, Jayakannan M (2015) Dual stimuli polysaccharide nanovesicles for conjugated and physically loaded doxorubicin delivery in breast cancer cells. *Nanoscale* 7:6636–6652
- [33] Xu H, Cao W, Zhang X (2013) Selenium-containing polymers: promising biomaterials for controlled release and enzyme mimics. *Acc Chem Res* 46:1647–1658
- [34] Huang S, Shao K, Liu Y, Kuang Y, Li J, An S, Guo Y, Ma H, Jiang C (2013) Tumor-targeting and microenvironment-

- responsive smart nanoparticles for combination therapy of antiangiogenesis and apoptosis. *ACS Nano* 7:2860–2871
- [35] Loh XJ (2013) Poly(DMAEMA-co-PPGMA): dual-responsive “reversible” micelles. *J Appl Polym Sci* 127:992–1000
- [36] Zhang M, Liu J, Kuang Y, Li Q, Zheng DW, Song Q, Chen H, Chen X, Xu Y, Li C, Jiang B (2017) Ingenious pH-sensitive dextran/mesoporous silica nanoparticles based drug delivery systems for controlled intracellular drug release. *Int J Biol Macromol* 98:691–700
- [37] Chen W, Hou Y, Tu Z, Gao L, Haag R (2017) pH-degradable PVA-based nanogels via photo-crosslinking of thermo-preinduced nanoaggregates for controlled drug delivery. *J Control Release* 259:160–167
- [38] Kanamala M, Wilson WR, Yang M, Palmer BD, Wu Z (2016) Mechanisms and biomaterials in pH-responsive tumour targeted drug delivery: a review. *Biomaterials* 85:152–167
- [39] Murthy N, Campbell J, Fausto N, Hoffman AS, Stayton PS (2003) Design and synthesis of pH-responsive polymeric carriers that target uptake and enhance the intracellular delivery of oligonucleotides. *J Control Release* 89:365–374
- [40] Du JZ, Du XJ, Mao CQ, Wang J (2011) Tailor-made dual pH-sensitive polymer-doxorubicin nanoparticles for efficient anticancer drug delivery. *J Am Chem Soc* 133:17560–17563
- [41] Qiao ZY, Qiao SL, Fan G, Fan YS, Chen Y, Wang H (2014) One-pot synthesis of pH-sensitive poly(RGD-co-bamino ester)s for targeted intracellular drug delivery. *Polym Chem* 5:844–853
- [42] Mukhopadhyay P, Chakraborty S, Bhattacharya S, Mishra R, Kundu PP (2015) pH-sensitive chitosan/alginate core-shell nanoparticles for efficient and safe oral insulin delivery. *Int J Biol Macromol* 72:640–648
- [43] Liu J, Huang Y, Kumar A, Tan A, Jin S, Mozhi A, Liang XJ (2014) pH-Sensitive nano-systems for drug delivery in cancer therapy. *Biotechnol Adv* 32:693–710
- [44] Li L, Knickelbein K, Zhang L, Wang J, Obrinské M, Ma GZ, Zhang L, Bitterman L, Du W (2015) Amphiphilic sugar poly(orthoesters) as pH-responsive nanoscopic assemblies for acidity-enhanced drug delivery and cell killing. *Chem Commun* 51:13078–13081
- [45] Gillies ER, Frechet JMJ (2005) pH-responsive copolymer assemblies for controlled release of doxorubicin. *Bioconjugate Chem* 16:361–368
- [46] Lee S, Saito K, Lee HR, Lee MJ, Shibasaki Y, Oishi Y, Kim BS (2012) Hyperbranched double hydrophilic block copolymer micelles of poly(ethylene oxide) and polyglycerol for pH-responsive drug delivery. *Biomacromolecules* 13:1190–1196
- [47] Li L, Xu Y, Milligan I, Fu L, Franckowiak EA, Du W (2013) Synthesis of highly pH-responsive glucose poly(orthoester). *Angew Chem Int Ed* 52:13699–13702
- [48] Yan G, Wang J, Qin J, Hu L, Zhang P, Wang X, Tang R (2017) Well-defined poly(ortho ester amides) for potential drug carriers: probing the effect of extra- and intracellular drug release on chemotherapeutic efficacy. *Macromol Biosci* 17:1600503
- [49] Yan G, Zha Q, Wang J, Wang X, Cheng X, Yao W, Tang R (2017) Dynamic, ultra-pH-sensitive graft copolymer micelles mediated rapid, complete destruction of 3-D tumor spheroids in vitro. *Polymer* 111:192–203
- [50] Yu M, Huang S, Yu KJ, Clyne AM (2012) Dextran and polymer polyethylene glycol (PEG) coating reduce both 5 and 30 nm iron oxide nanoparticle cytotoxicity in 2D and 3D cell culture. *Int J Mol Sci* 13:5554–5570
- [51] Zhang S, Yang K, Feng L, Liu Z (2011) In vitro and in vivo behaviors of dextran functionalized grapheme. *Carbon* 49:4040–4049
- [52] Hu Y, He L, Ding J, Sun D, Chen L, Chen X (2016) One-pot synthesis of dextran decorated reduced graphene oxide nanoparticles for targeted photo-chemotherapy. *Carbohydr Polym* 144:223–229
- [53] Shaterabadi Z, Nabiyouni G, Soleymani M (2017) High impact of in situ dextran coating on biocompatibility, stability and magnetic properties of iron oxide nanoparticles. *Mater Sci Eng C* 75:947–956
- [54] Balakrishnan B, Soman D, Payanam U, Laurent A, Labarre D, Jayakrishnan A (2017) A novel injectable tissue adhesive based on oxidized dextran and chitosan. *Acta Biomater* 53:343–354
- [55] Chen X, Yao X, Chen L (2015) Intracellular pH-sensitive dextran-based micelles as efficient drug delivery platforms. *Polym Int* 64:430–436
- [56] Tang R, Ji W, Wang C (2010) Amphiphilic block copolymers bearing ortho ester side-chains: pH-dependent hydrolysis and self-assembly in water. *Macromol Biosci* 10:192–201
- [57] Zhou X, Luo S, Tang R, Wang R, Wang J (2015) Diblock copolymers of polyethylene glycol and a polymethacrylamide with side-chains containing twin ortho ester rings: synthesis, characterization, and evaluation as potential pH-responsive micelles. *Macromol Biosci* 15:385–394
- [58] Wang X, Tang H, Wang C, Zhang J, Wu W, Jiang X (2016) Phenylboronic acid-mediated tumor targeting of chitosan nanoparticles. *Theranostics* 6:1378–1392
- [59] Wang X, Yang C, Zhang Y, Zhen X, Wu W, Jiang X (2014) Delivery of platinum(IV) drug to subcutaneous tumor and lung metastasis using bradykinin-potentiating peptide-decorated chitosan nanoparticles. *Biomaterials* 35:6439–6453

- [60] Yu M, Zhang L, Wang J, Tang R, Yan G, Cao Z, Wang X (2016) Acid-labile poly(ortho ester amino alcohols) by ring-opening polymerization for controlled DNA release and improved serum tolerance. *Polymer* 96:146–155
- [61] Tang R, Ji W, Wang C (2011) Synthesis and characterization of new poly(ortho ester amidine) copolymers for non-viral gene delivery. *Polymer* 52:921–932
- [62] Lai J, Xu Z, Tang R, Ji W, Wang R, Wang J (2014) PEGylated block copolymers containing tertiary amine side-chains cleavable via acid-labile ortho ester linkages for pH-triggered release of DNA. *Polymer* 55:2761–2771
- [63] Gaio E, Scheglmann D, Reddi E, Moret F (2016) Uptake and photo-toxicity of Foscan[®], Foslip[®] and Fospeg[®] in multicellular tumor spheroids. *J Photochem Photobiol B* 161:244–252
- [64] Fu S, Yang G, Wang J, Wang X, Cheng X, Zha Q, Tang R (2017) pH-sensitive poly(ortho ester urethanes) copolymers with controlled degradation kinetic: synthesis, characterization, and in vitro evaluation as drug carriers. *Eur Polym J* 95:275–288
- [65] Yang G, Wang X, Fu S, Tang R, Wang J (2017) pH-triggered chitosan nanogels via an ortho ester-based linkage for efficient chemotherapy. *Acta Biomater* 60:232–243